Contributions of IR thermography and X-ray tomography to the fatigue characterization of elastomeric materials

Yann Marco, Isaure Masquelier, Vincent Le Saux, Sylvain Calloch, Bertrand Huneau, Pierre Charrier

Fatigue damage in carbon black filled natural rubber investigated by X-ray microtomography and scanning electron microscopy

B. Huneau
LUNAM Université, Ecole Centrale de Nantes, Institut de Recherche en Génie Civil et Mécanique (GeM), UMR CNRS 6183, Nantes, France

I. Masquelier & Y. Marco
ENSTA Bretagne, Laboratoire Brestois de Mécanique des Structures (LBMS), EA 4325, Brest, France

O. Brzokewicz & P. Charrier
TrelleborgVibracoustic Group, Modyn, Carquefou, France

ABSTRACT: An experimental procedure that combines scanning electron microscopy (SEM) observations and X-ray microtomography is applied in order to study the damage mechanisms and the damage evolution along the fatigue lifetime of a carbon black filled natural rubber (NR). It is shown that internal and external cracks typically initiate on carbon black agglomerates, most of them being in the range of 10 to 20 μm in size. Moreover, the parting line of the injection molded fatigue specimens appears to be a particular site for the initiation of external cracks, generally with the additional contribution of carbon black agglomerates. A quantitative analysis of both internal and external fatigue cracks is performed and shows that fatigue damage occurs mainly at the surface of the rubber samples. The evolution of the number of internal and external cracks has a quasi-linear behavior with respect to the number of fatigue cycles.

1 INTRODUCTION

The damage induced by fatigue loading in rubber can be investigated by several experimental techniques. For example, scanning electron microscope (SEM) is a powerful tool to study fatigue fracture surfaces in order to identify crack initiation sites or to analyze crack propagation stage (Le Cam 2005, Saintier et al. 2006, Hainsworth 2007, Flamm et al. 2011, Le Cam et al. 2013). SEM has also been used to study the fatigue crack growth mechanism in carbon black filled natural rubber (NR) on a stretched sample containing a fatigue crack (Le Cam et al. 2004) or during in-situ fatigue tests (Beurrot et al. 2010). This useful technique is however limited to investigate fatigue damage because it only gives surface information, which is a strong limitation since damage can occur in the volume of the material. To overcome this drawback, some authors have recently used X-ray computed microtomography, which allows to visualize the microstructure inside the rubber parts or specimens (Le Gorju Jago 2012). For instance, this technique was used for a carbon black filled NR (Le Gorju Jago 2007) and a chloroprene rubber (CR) (Le Saux et al. 2011). In addition, Le Saux et al. (2010) showed that results from microtomography associated with data obtained with a heat build-up protocol can provide a criterion based on critical energy in order to predict the fatigue lifetime.

The objective of the present study is to follow the damage inside and at the surface of a carbon black filled natural rubber during interrupted fatigue tests by using both SEM and microtomography techniques.

The experimental procedure will be first detailed in section 2. Afterwards, the results concerning the mechanisms of fatigue crack initiation and the quantitative evolution of the cracks will be presented and discussed in section 3.

2 EXPERIMENTAL PROCEDURE

2.1 *Material*

The compound is a natural rubber (NR) filled with carbon black (CB) N550 and sulphur cured. The chemical composition is given in Table 1.

Table 1. Composition of the NR.

Compound	Content
	parts per hundred rubber (phr)
NR gum	100
Carbon Black N550	43
Sulphur	1.8
CBS	2.5
Zinc oxide	5.0

Regarding its CB content, the material is referred to as NR43 in the following. The distribution of the size of the CB agglomerates is determined through a dispergrader analysis. The maximum of the size distribution function is around 10 μm.

2.2 *Fatigue tests*

Fatigue tests are performed on hourglass-shaped specimens (this geometry is referred to as AE2 in the text). The median zone of those specimens is 10 mm in diameter. Part of the fatigue tests was conducted at TrelleborgVibracoustic on a specific device and the other was performed at Ecole Centrale Nantes on an Instron E10000 electropulse machine.

All the fatigue tests are monitored with prescribed displacement and for a minimum displacement equal to zero. The frequency of the tests is in the range of 1 to 5 Hz. By using 25 specimens, a Wöhler curve (not shown here) is plotted with the maximum principal strain (calculated at the surface of the median zone of the sample for the maximum displacement) as a function of the number of cycles corresponding to the end-of-life of the specimens. This number is called Ni and is detected by a loss of the specimen stiffness, see Ostoja-Koczynski et al. (2003) for the details. On AE2 samples, it corresponds to the presence of one or more large cracks measuring approximately 1 or 2 mm. This Wöhler curve is used as a reference to define the strain level and the number of cycles for each sequence of the interrupted fatigue tests.

Two protocols were used for the interrupted fatigue tests:

– protocol 1: for each strain level, the same sample is followed along the fatigue life,

– protocol 2: many samples are subjected to fatigue and stopped at a certain ratio of Ni. This protocol corresponds to the one proposed by Le Saux et al. (2011).

In the present paper, only the results of two representative samples subjected to protocol 1 are presented (see Table 2). For these two samples, the fatigue test is interrupted every 10,000 cycles.

Table 2. Fatigue tests

Sample	maximum strain level	maximum number of cycles
	%	
NR43-s1	100	130,000
NR43-s2	150	40,000

2.3 *Tomography*

The X-ray microtomography analysis is performed with an X-radia MicroXCT-400 device. During the acquisition of the images, fatigue samples are stretched of 3 mm (it corresponds roughly to a maximal strain of 50% at the surface of the median zone of the specimens) to slightly open the existing cracks. In order to minimize the damage due to the exposure to X-rays and to obtain a good contrast, the acceleration voltage of the tube is limited to 40 kV. Exposure time for each projection is then adjusted to 30 seconds to ensure a sufficient intensity on the CCD detector. Each voxel is 8.6 x 8.6 x 8.6 µm in size. This resolution requires 1650 projections, which leads to an acquisition time of 15 hours and to a file size of 3.6 gigabytes.

The reconstructed file can be analyzed by the microtomograph viewer, which provides 2D slices and a 3D view. Figure 1 gives an example of this 3D representation for an AE2 sample after a fatigue test. On this view, many external cracks are visible. It shows that microtomography can also be used to investigate the external cracks.

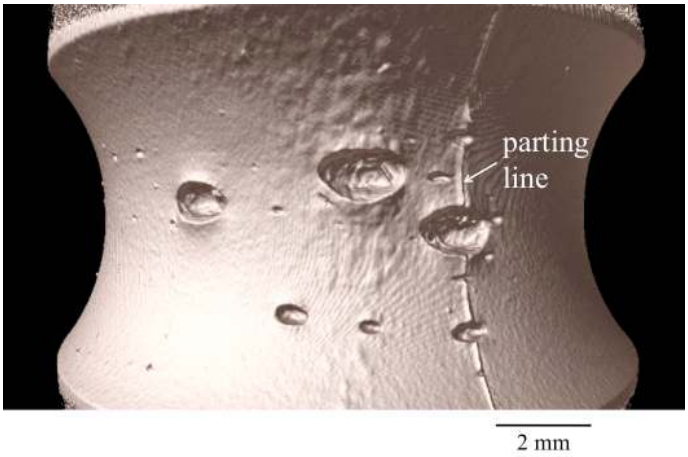

Figure 1. Example of a 3D view from microtomography showing external cracks (NR43-s1 at 100,000 cycles).

Reconstructed files can also be analyzed by using the software ParaView devoted to image analysis and visualization. This software allows to quantify the number and the volume of internal cracks by using the following method:

– On the histogram of grey levels, dark voxels are considered as voids.

– Regions that contain connected voids are identified. Each region is counted as one crack.

– Considering the volume of one voxel, the number of voxels per region and the number of regions, the total volume associated with internal cracks is calculated.

2.4 *Scanning Electron Microscope (SEM)*

The SEM investigations are performed with a JEOL 6060-LA. The acceleration voltage is 20 kV and the damage caused by the electrons is limited by a short time exposure and a low magnification. The images are taken by using the secondary electrons signal. The chemical composition of dense inclusions can be determined thanks to an Energy Dispersive Spectrometer (EDS) of X-rays associated with the SEM.

In the present study, SEM is used to analyze the crack initiation mechanisms by observing either the fracture surfaces or the surface of fatigue specimens for an extension of 3 mm.

3 RESULTS AND DISCUSSION

3.1 *Initiation mechanisms of fatigue cracks*

The observations performed on samples NR43-s1 (maximal strain of 100 %) and NR43-s2 (maximal strain of 150 %) did not reveal any effect of the strain level on the fatigue crack initiation mechanisms. Consequently, these mechanisms are presented independently from the strain level.

A large majority of the inclusions inducing a fatigue crack initiation are CB agglomerates. Thus, only results concerning CB agglomerates are reported here. Rarely, the inclusions responsible for the crack initiation are oxides with an approximate size of 50 µm. They usually contain silicium and oxygen (SiO_2) and often other elements (Mg, Na, Ca, K…) that seem to be also associated with oxygen, in the form of oxides. Until now, their origin remains unclear as they may come either from the gum or from the process. In the present study, no zinc oxide (ZnO) particles were found to lead to fatigue crack initiation.

3.1.1 *Internal cracks*

As previously explained, internal defects or cracks can only be detected by tomography. Figure 2a shows a 2D slice of a fatigued sample with one internal defect (with 2 voids) and 3 external cracks. Generally, few internal voids are detected in the volume of the samples and they are located close to the surface (most of them are at a maximum distance of 1 mm from the surface), which is rather logical if one considers the geometry of the specimen and the expected mechanical fields. Around the biggest CB agglomerates (only one or two per sample with an approximate size of 100 to 150 µm) an interface failure mechanism occurs. The density of the CB agglomerates being very close to the one of the rubber matrix, this failure mechanism can only be detected when the samples are stretched. This can be seen in Figure 2b, where two voids are visible at the pole of the CB agglomerate. One should note that this kind of defect does not lead automatically to the formation of a large crack. However, in section 3.2 those voids (cavities around CB agglomerates) will be considered as cracks. Sometimes, no CB agglomerate seems to be responsible for internal cracks on tomographic 2D slices, as shown in Figure 2c.

Figure 3a shows SEM observations of two internal circular cracks of 100 µm in diameter that initiated on CB agglomerates. In that case, the size of the agglomerates is in the range of 10 – 20 µm. It explains that they can be hardly detected with the microtomography, for which we recall that the spatial resolution is 8.6 µm. Figures 3b and 3c show 2D slices obtained from microtomography, each of them containing one of those two cracks before failure. They cannot appear on the same slice since they are clearly not at the same height.

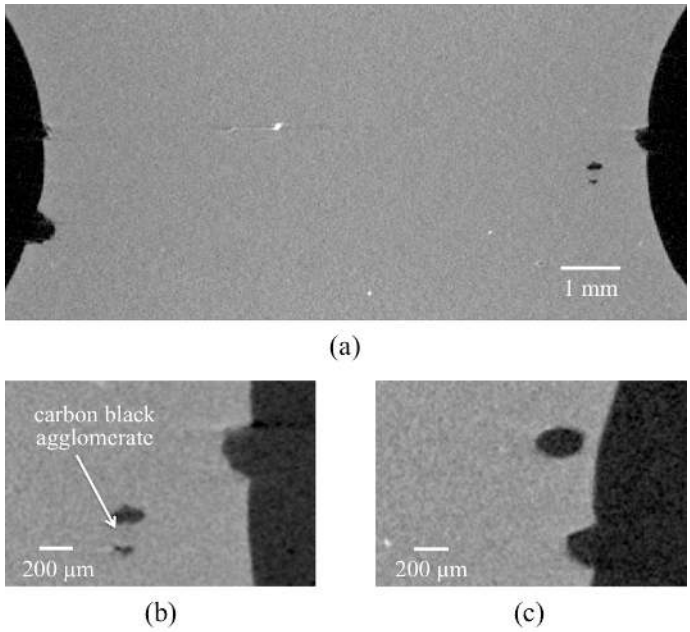

Figure 2. 2D slices from microtomography showing: (a) internal voids and external cracks (NR43-s1 at 90,000 cycles), (b) higher magnification picture showing the CB agglomerate; (c) internal crack without any visible inclusion (NR43-s2 at 40,000 cycles).

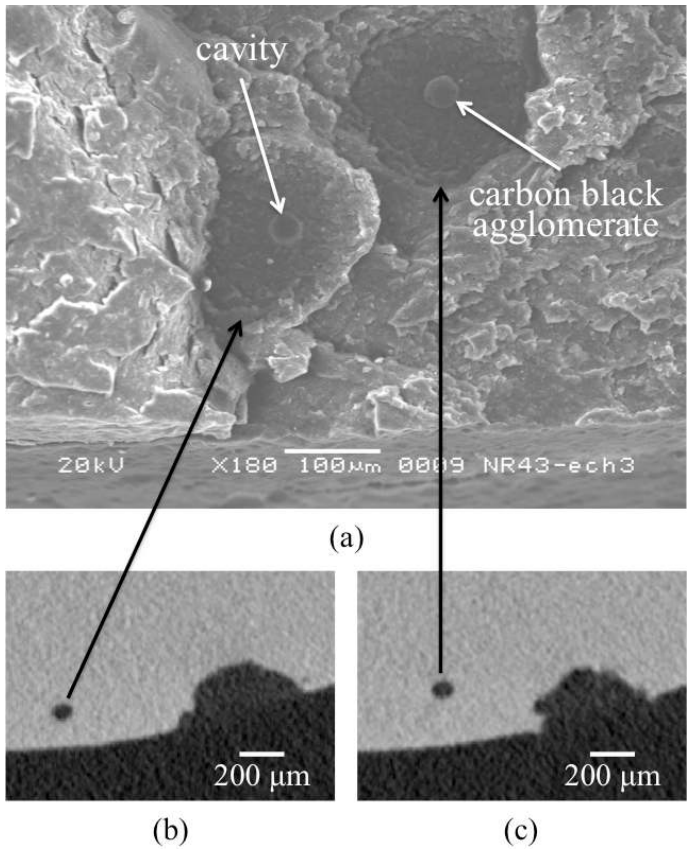

Figure 3. (a) Internal circular cracks initiated on CB agglomerates. The initiation site of the left hand crack appeared as a cavity, the CB agglomerate being on the other fracture surface (NR43-s2 after failure); (b) and (c) are the corresponding 2D slices at 40,000 cycles (before failure).

3.1.2 *External cracks*

External cracks can be seen on 3D tomographic view (see Fig.1 for example) but the spatial resolution is too low to clearly analyze the initiation site, so SEM observations are required. Figure 4a pre-

sents such an external crack after 40,000 cycles for the sample NR43-s2. The white arrow indicates the CB agglomerate. Figures 4b and 4c illustrate the early stages of this initiation mechanism for two other cracks on the same sample, but after only 10,000 cycles. To the authors' knowledge, this kind of mechanism was never reported in the literature.

Our observations also reveal that the parting line is a preferential site for crack initiation, as it can be seen in Figure 5. The reader can also refer to Figure 1 in which a few cracks are perfectly centered with respect to the parting line, suggesting this type of initiation mechanism. Figure 5a shows a crack where neither CB agglomerates nor any type of inclusion is visible, but one should note that an inclusion could have been removed (if the chemical bond between this hypothetical inclusion and the rubber was too weak). Nevertheless, Figure 5b clearly shows a crack initiation occurring on a CB agglomerate. This agglomerate seems to be "wedged" at the beginning of burr. As illustrated in Figure 5c, we have also observed some cracked parting line where small CB agglomerates are embedded in the burr and could be responsible for the crack initiation.

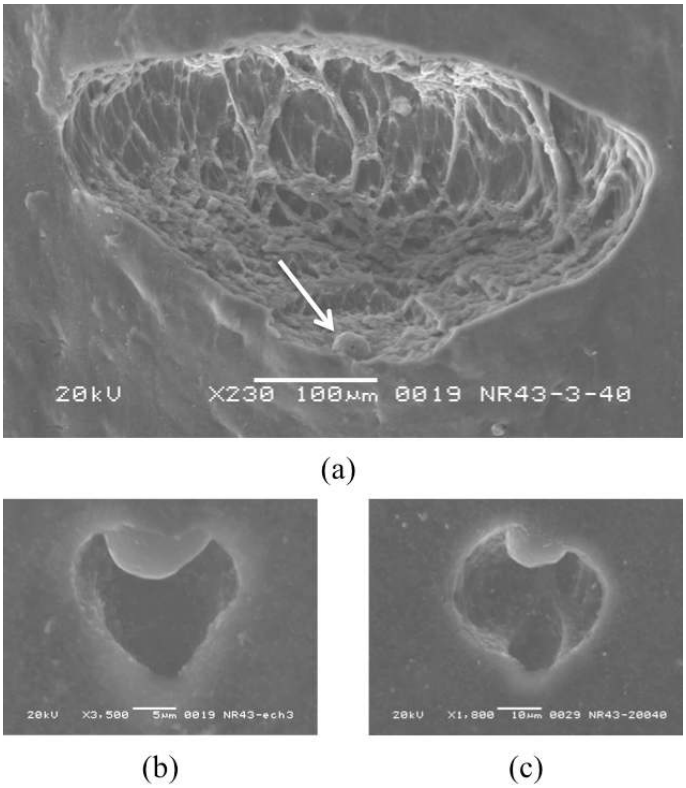

Figure 4. (a) External crack with the CB agglomerate responsible for its initiation indicated with the white arrow (NR43-s2 at 40,000 cycles); (b) and (c) illustrate the early stages of the type of initiation mechanism for two other external cracks (NR43-s2 at 10,000 cycles).

3.2 *Evolution of the number of cracks*

Thanks to the microtomography analysis performed at each interruption, it is possible to follow the number of internal and external cracks.

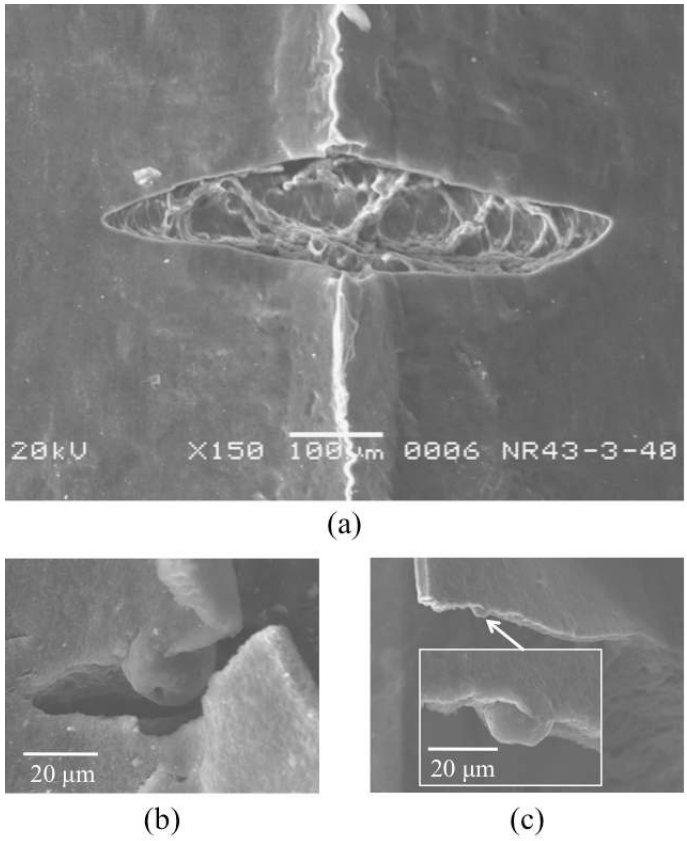

Figure 5. External cracks initiated at the parting line: (a) no inclusion is visible (NR43-s2 at 40,000 cycles); (b) CB agglomerate "wedged" at the beginning of burr and (c) CB agglomerate located in the burr (NR43-s1 at 130,000 cycles).

Figure 6 illustrates the evolution of internal cracks (that also includes voids at the pole of large CB agglomerates). The first comment on this curve is that the number of internal cracks detected remains very low: less than 10 at 100,000 cycles.

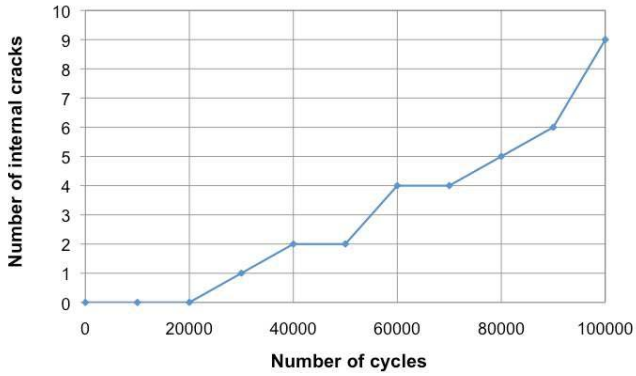

Figure 6. Number of internal cracks at a maximal strain of 100% (NR43-s1) during the fatigue test.

By using the method described in section 2.3, the volume corresponding to internal cracks is computed and shown in Figure 7. The evolution is no more quasi-linear, which demonstrates that the cracks are growing. The decrease of volume between 90,000 and 100,000 cycles is due to the fact that a large internal crack turns into an external one when it

reaches the surface. Figure 8 illustrates this mechanism. This is not detected in Figure 6 because the "disappearance" of this internal crack is compensated by the appearance of four new cracks.

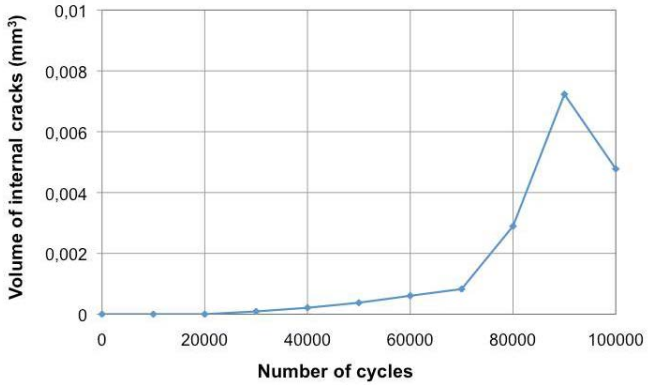

Figure 7. Volume of internal cracks at a maximal strain of 100% (NR43-s1) during the fatigue test.

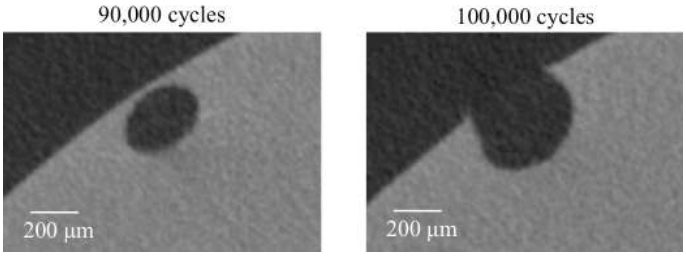

Figure 8. An internal crack becomes an external crack between 90,000 and 100,000 cycles (NR43-s1).

The external cracks were also counted, simply by using the viewer of the microtomograph. Figure 9 shows the surface damage evolution of a particular zone, which has a surface of approximately 1 mm^2, from 40,000 to 130,000 cycles (sample NR43-s1). This kind of visualization is very useful to detect the initiation of surface cracks and to follow their evolution.

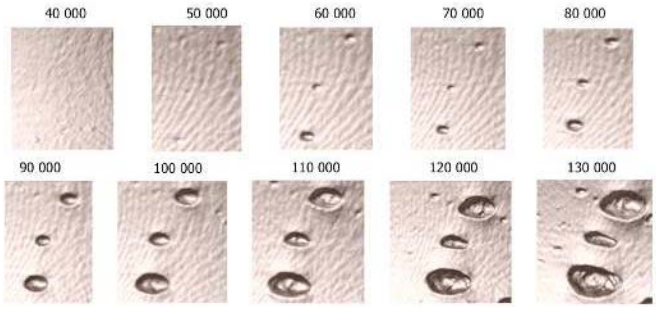

Figure 9. Evolution of external cracks on a fixed area; the number above each picture is the number of cycles.

Figure 10 gives the evolution of the number of external cracks with the number of cycles. This evolution is very regular as it was already observed for the internal cracks: from 20,000 cycles it has a quasi-linear behavior. This quantitative analysis confirms that the number of external cracks is higher than the number of internal cracks: at 100.000 cycles, it is 5 times more for NR43-s1 (maximum strain of 100%).

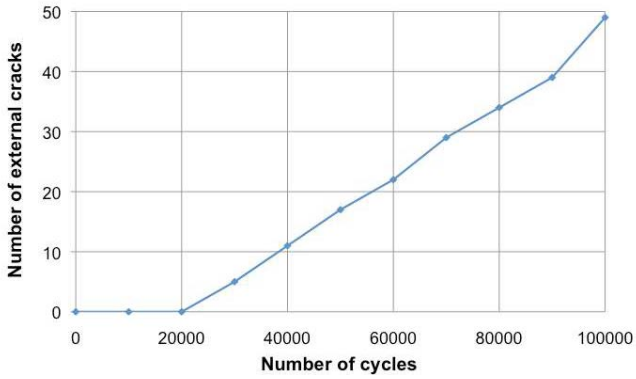

Figure 10. Number of external cracks at a maximal strain of 100% (NR43-s1) during the fatigue test.

3.3 *Discussion*

Previous studies from the literature reported three main fatigue crack initiation mechanisms involving inclusions in rubber: interface failure between one inclusion and the matrix, either by debonding or by cavitation very close to the interface, (Le Cam 2005, Saintier et al. 2006, Le Saux et al. 2011, Le Cam et al. 2013), inclusion fracture (Le Cam 2005, Le Saux et al. 2011, Le Cam et al. 2013) and cavitation between two or more close inclusions (Le Saux et al. 2011, Le Gorju Jago 2007). Those mechanisms correspond to the ones previously described by Gent & Park (1984), who used glass beads in various rubbers. In the present study, only the interface failure mechanism between isolated inclusions and the matrix is clearly seen. It concerns one or two large CB agglomerates in the volume per sample, but they do not control the final fracture of the sample, probably because they are too few and they are not located in the region with the highest strains. Most of the time, this interface failure mechanism occurs at the surface (external cracks) or close to the surface (internal cracks) on CB agglomerates being in the range of 10 to 20 µm, more rarely on oxides. These oxides are not ZnO inclusions that were seen to play a major role in another CB filled NR (Le Gorju Jago 2007). The smooth surface of the CB agglomerates revealed by SEM observations (see Figs 4-5) would suggest that the interface failure is rather due to a debonding mechanism than to a cavitation mechanism close to the interface. The parting line of fatigue specimens also plays an important role on the initiation of fatigue cracks, but this type of initiation often involves CB agglomerates too.

Concerning the location of the fatigue cracks and their density, it appears that they mostly occur at the surface of the specimens, which was not the case in some previously cited works. Indeed, Le Cam (2005, 2013) reported that the initiation generally takes

place at a distance of 200 to 600 µm from the surface. This so-called "subsurface initiation" is supposed to be due to the curing operation that would induce a "skin effect", the skin having different mechanical properties compared to the core of the samples because of a different thermal history. In the present study, some subsurface crack initiations are also observed and they correspond to the internal cracks presented in section 3.1.1. The higher importance of internal cracks initiation in some previous studies could also due to the presence of numerous large inclusions (bigger than 50 µm), as it was the case for the chloroprene rubber (CR) filled mainly with silica and studied by Le Saux et al. (2011). Here, the low number of internal cracks suggests that the compound is rather well dispersed: each sample contains only one or two CB agglomerates larger than 100 µm and no large ZnO inclusions that could have played a major role in fatigue damage. It also does not contain enough inclusions aligned with the loading direction to promote the crack initiation between inclusions as it was observed in other studies (Le Saux et al. 2011, Le Gorju Jago 2007).

Finally, the mechanisms of fatigue crack initiation as well as the location and the number of fatigue cracks seem to be strongly related to the rubber processing (mixing, injection, curing) that controls the size and the spatial distribution of the inclusions.

4 CONCLUSION

An experimental procedure associating X-ray microtomography and SEM allows to follow fatigue damage along fatigue tests. By using these two techniques, we are able to consider both internal and external cracks and to study the fatigue crack initiation mechanisms.

In the considered carbon black filled NR (NR43), the initiation mainly occurs on CB agglomerates with a size of 10 to 20 µm. Most of the cracks initiate at the surface and the rest at the subsurface. The parting line of the specimens has also an influence on the fatigue crack initiation.

This procedure is currently applied to other materials (NR or other matrixes with different CB contents) in order to correlate the fatigue lifetime, and the scattering of the end-of-life results, to the fatigue damage scenarios, which are strongly related to microstructural heterogeneities.

ACKNOWLEDGMENTS

The authors would like to thank the ANR for its financial support (ANR–2010–RMNP-010-01) and all the partners of the PROFEM project: ENSTA Bretagne, TrelleborgVibracoustic, UBS, LRCCP and ECN.

REFERENCES

Beurrot, S., B. Huneau & E. Verron 2010. In situ SEM study of fatigue crack growth mechanism in carbon black-filled natural rubber. *Journal of Applied Polymer Science,* 117, 1260-1269.

Flamm, M., J. Spreckels, T. Steinweger & U. Weltin 2011. Effects of very high loads on fatigue life of NR elastomer materials. *International Journal of Fatigue,* 33, 1189-1198.

Gent, A. N. & B. Park 1984. Failure processes in elastomers at or near a rigid spherical inclusion. *Journal of Materials Science,* 19, 1947-1956.

Hainsworth, S. V. 2007. An environmental scanning electron microscopy investigation of fatigue crack initiation and propagation in elastomers. *Polymer Testing,* 26, 60-70.

Le Cam, J.-B. 2005. *Endommagement en fatigue des élastomères.* PhD Thesis, Ecole Centrale de Nantes.

Le Cam, J. B., B. Huneau & E. Verron 2013. Fatigue damage in carbon black filled natural rubber under uni- and multiaxial loading conditions. *International Journal of Fatigue,* to be published.

Le Cam, J. B., B. Huneau, E. Verron & L. Gornet 2004. Mechanism of fatigue crack growth in carbon black filled natural rubber. *Macromolecules,* 37, 5011-5017.

Le Gorju Jago, K. 2007. Fatigue life of rubber components: 3D damage evolution from X-ray computed microtomography. *In:* A. Boukamel, L. Laiarinandrasana, S. Méo & E. Verron (eds), *Constitutive Models for Rubber V*, 2007 Paris. Taylor & Francis/Balkema, 173-177.

Le Gorju Jago, K. 2012. X-ray computed microtomography of rubber. *Rubber Chemistry and Technology,* 85, 387-407.

Le Saux, V., Y. Marco, S. Calloch & P. Charrier 2011. Evaluation of the Fatigue Defect Population in an Elastomer Using X-Ray Computed Micro-Tomography. *Polymer Engineering and Science,* 51, 1253-1263.

Le Saux, V., Y. Marco, S. Calloch, C. Doudard & P. Charrier 2010. Fast evaluation of the fatigue lifetime of rubber-like materials based on a heat build-up protocol and micro-tomography measurements. *International Journal of Fatigue,* 32, 1582-1590.

Ostoja-Kuczynski, E., P. Charrier, E. Verron, G. Marckmann, L. Gornet & G. Chagnon 2003. Crack initiation in filled natural rubber: experimental database and macroscopic observations. *In:* J. Busfield & A. Muhr (eds), *Constitutive Models for Rubber III*, 2003 London. Taylor & Francis, 41-47.

Saintier, N., G. Cailletaud & R. Piques 2006. Crack initiation and propagation under multiaxial fatigue in a natural rubber. *International Journal of Fatigue,* 28, 61-72.